Vehicle System Dynamics
Vol. 44, No. 5, May 2006, 387–406

Taylor & Francis
Taylor & Francis Group

Control of a hydraulically actuated continuously variable transmission

MICHIEL PESGENS*†§, BAS VROEMEN†, BART STOUTEN‡, FRANS VELDPAUS‡ and MAARTEN STEINBUCH‡

†Drivetrain Innovations b.v., Horsten 1, 5612 AX, The Netherlands
‡Technische Universiteit Eindhoven, PO Box 513, 5600 MB Eindhoven, The Netherlands

Vehicular drivelines with hierarchical powertrain control require good component controller tracking, enabling the main controller to reach the desired goals. This paper focuses on the development of a transmission ratio controller for a hydraulically actuated metal push-belt continuously variable transmission (CVT), using models for the mechanical and the hydraulic part of the CVT. The controller consists of an anti-windup PID feedback part with linearizing weighting and a setpoint feedforward. Physical constraints on the system, especially with respect to the hydraulic pressures, are accounted for using a feedforward part to eliminate their undesired effects on the ratio. The total ratio controller guarantees that one clamping pressure setpoint is minimal, avoiding belt slip, while the other is raised above the minimum level to enable shifting. This approach has potential for improving the efficiency of the CVT, compared to non-model based ratio controllers. Vehicle experiments show that adequate tracking is obtained together with good robustness against actuator saturation. The largest deviations from the ratio setpoint are caused by actuator pressure saturation. It is further revealed that all feedforward and compensator terms in the controller have a beneficial effect on minimizing the tracking error.

Keywords: Continuously variable transmission; Feedforward compensation; Feedback linearization; Hydraulic actuators; Constraints

1. Introduction

The application of a continuously variable transmission (CVT) instead of a stepped transmission is not new. Already in the 50s Van Doorne introduced a rubber V-belt CVT for vehicular drivelines. Modern, electronically controlled CVTs make it possible for any vehicle speed to operate the combustion engine in a wide range of operating points, for instance in the fuel optimal point. For this reason, CVTs get increasingly important in hybrid vehicles, see for example [1–3]. Accurate control of the CVT transmission ratio is essential to achieve the intended fuel economy and, moreover, ensure good driveability.

The ratio setpoint is generated by the hierarchical (coordinated) controller of figure 1. This controller uses the accelerator pedal position as the input and generates setpoints for the local controllers of the throttle and of the CVT.

*Corresponding author. Email: pesgens@dtinnovations.nl
§Michiel Pesgens was previously affiliated with Technische Universiteit Eindhoven.

Vehicle System Dynamics
ISSN 0042-3114 print/ISSN 1744-5159 online © 2006 Taylor & Francis
http://www.tandf.co.uk/journals
DOI: 10.1080/00423110500244088

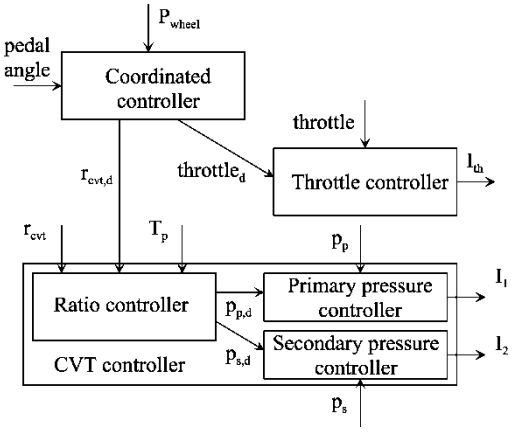

Figure 1. Hierarchical powertrain control.

The CVT and its hydraulic actuation system are depicted in figures 2, 3. The hydraulic system not only has to guarantee good tracking behavior of the CVT but also has to realize clamping forces that, on the one hand, are high enough to prevent belt slip but, on the other hand, are as low as possible to maximize the transmission efficiency and to reduce wear. In practice, the clamping forces levels are kept at levels that avoid belt slip at all times, while still maintaining an acceptable degree of transmission efficiency.

The main focus of this paper is on the ratio control of the CVT, using the hydraulic actuation system of figure 3. The presented control concept is based on the work of [3, 4]. It enables tracking of the ratio setpoint, while guaranteeing at least one of the two pulley pressure setpoints to be equal to its lower constraint. Even though the controller effectively changes from controlling one of the two pressures to the other, no actual switching between different controllers takes place. Among the approaches seen in the literature, some incorporate a switching algorithm [3, 5], whereas others control only one of the two (usually the primary) pressures [6, 7]. Although the former approach cannot guarantee one of the two pressures to be equal to its lower constraint, the latter cannot explicitly prevent the uncontrolled pressure to stay above its lower constraint.

The rest of this paper is organized as follows. First, a mathematical model is derived for the mechanical part of the CVT in section 2. Next, in section 3, the hydraulic part is modeled. The physical constraints, imposed by the hydraulic system, are discussed in section 4. These constraints are taken into account by the CVT ratio controller, that is developed in section 5

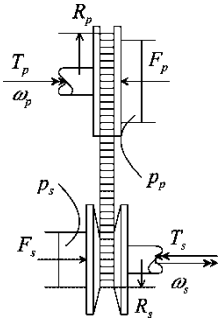

Figure 2. Variator.

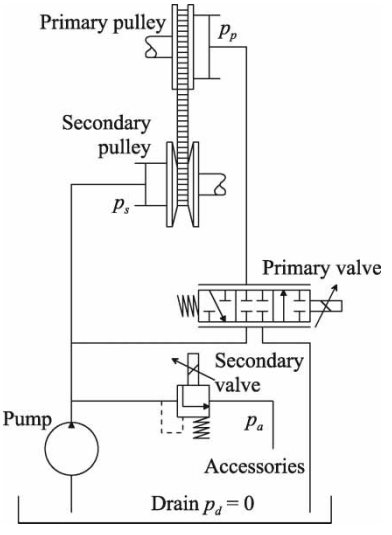

Figure 3. Variator with hydraulic system.

and is based on the earlier derived models for the mechanical and the hydraulic CVT parts. The tracking performance of this controller is experimentally evaluated in section 6. Finally, section 7 gives some concluding remarks.

2. The pushbelt CVT

The CVT (figure 2) considered here is equipped with a Van Doorne metal pushbelt. This belt consists of a large number (around 350) of V-shaped steel block elements, held together by a number (between 9 and 12) of thin steel tension rings. The belt runs on two pulleys, namely the primary pulley at the engine side and the secondary pulley at the wheel side. Each pulley consists of one axially fixed and one moveable sheave, operated by means of a hydraulic cylinder. The cylinders can be pressurized, generating axial forces (clamping forces or thrusts) on the belt, necessary for transmission of torque (without macro-slip of the belt) and for ratio change. Here the distinction is made between micro-slip, needed for torque transfer between belt and pulleys, and macro-slip, which should be avoided at all times for its negative effect on efficiency and especially the risk of severe belt and pulley wear [8].

The bounded transmission ratio $r_{\mathrm{cvt}} \in [r_{\mathrm{cvt,LOW}}, r_{\mathrm{cvt,OD}}]$ is defined here as the ratio of secondary pulley speed ω_{s} over primary pulley speed ω_{p}, so:

$$r_{\mathrm{cvt}} = \frac{\omega_{\mathrm{s}}}{\omega_{\mathrm{p}}} \tag{1}$$

In deriving the variator model, it has been assumed that the pulleys are rigid and perfectly aligned, and that the V-shaped blocks are rigid and the steel rings are inextensible. The belt is assumed to run in perfect circles on the pulleys. Further, it has been assumed that the clamping forces are large enough to prevent macro belt slip. The effects of micro-slip are relatively small with respect to the ratio change behavior of the CVT, and are, therefore, neglected in the model. The power transmission between the belt and the pulleys is modeled as Coulomb friction (which is assumed in the majority of CVT variator research [3]).

Using these assumptions, the running radii R_p and R_s of the belt on the primary and secondary pulleys are functions of the ratio r_{cvt} only and are related by:

$$R_p = r_{cvt} \cdot R_s \tag{2}$$

The axial position s_α ($\alpha = p$ for the primary pulley, $\alpha = s$ for the secondary one) of the moveable pulley sheave of pulley α is also completely determined by the ratio r_{cvt}. Denoting the taper angle of the conical sheaves by φ (see figure 4), it is easily seen that s_α is given by:

$$s_\alpha = 2 \cdot \tan(\varphi) \cdot (R_\alpha - R_{\alpha,\min}) \tag{3}$$

Subscript 'max' (or 'min') implies the maximum (or minimum) value possible, e.g. $X_{max} = \max(X)$, unless stated otherwise. Differentiation with respect to time yields the axial velocity $\dot{s}_\alpha$ of the moveable sheave of pulley α

$$\dot{s}_\alpha = \nu_\alpha(r_{cvt}) \cdot \dot{r}_{cvt} \tag{4}$$

where the function ν_α follows from the geometry of the variator.

Assuming that the radial friction force component between the pulley and the belt is zero, the critical pulley clamping force (equal for both pulleys, neglecting the variator's efficiency) is given by references [3, 5] (for pulley α):

$$F_{crit} = \frac{\cos(\varphi) \cdot |T_\alpha|}{2 \cdot \mu \cdot R_\alpha} \tag{5}$$

where T_α is the net transmitted torque between belt and pulley and μ is the coulomb friction coefficient between pulleys and belt. The factor 2 appears, as there are two friction surfaces between pulley and belt.

Radial forces between belt and pulleys can be mainly contributed to centrifugal forces and Coriolis forces. In the detailed thrust force model of ref. [9], it is reported that even if the sliding angle (and hence the friction force angle) ξ between the belt path and the friction force vector changes along the pulley circumference, its value converges rapidly towards values less than 10°. As a result, the angle is assumed zero. The friction force angle ξ would enter into equation (5) as a multiplication factor $\cos(\xi)$, which rapidly converges to 1 for small angles.

For the choice of μ, a worst-case approach is applied. It is chosen as the maximum of the traction curve (of which several have been presented in ref. [10]), which is the point of transition from micro-slip to macro-slip. The lowest value of all the maxima found in ref. [10], as well as in ref. [8] (for both very similar variators) is 0.09, the value of μ that has been used here.

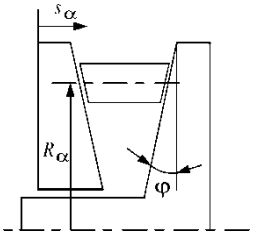

Figure 4. Pulley sheave definitions.

The torque ratio τ_α is the ratio of transmitted torque and maximally transmittable torque without belt slip for pulley α:

$$\tau_\alpha = \frac{T_\alpha}{T_{\alpha,\max}} = \frac{\cos(\varphi) \cdot T_\alpha}{2 \cdot \mu \cdot R_\alpha \cdot F_\alpha} \tag{6}$$

As in a practical vehicle application a good estimate of the torques acting on the secondary pulley is not available, the following modified torque ratio is introduced:

$$\tau_{\mathrm{s}}' = \frac{\cos(\varphi) \cdot \hat{T}_{\mathrm{p}}}{2 \cdot \mu \cdot R_{\mathrm{p}} \cdot F_{\mathrm{s}}} \tag{7}$$

The estimated primary transmitted torque $\hat{T}_{\mathrm{p}}$ can be obtained from the dynamic driveline equations together with engine and torque converter characteristics (also see section 4). In case of a perfect torque estimation, i.e. $\hat{T}_{\mathrm{p}} = T_{\mathrm{p}}$, it is easily seen that (using equation (6)):

$$\tau_{\mathrm{s}}' = \frac{P_{\mathrm{p}}}{P_{\mathrm{s}}} \cdot \tau_{\mathrm{s}} \tag{8}$$

with transmitted power $P_\alpha = T_\alpha \cdot \omega_\alpha$. As it has been assumed that $P_{\mathrm{p}} = P_{\mathrm{s}}$, the modified torque ratio becomes equal to the torque ratio for the secondary pulley.

An important part of the model for the mechanical part of the CVT is the sub-model for the rate of ratio change as a function of, for instance, the clamping forces. Sub-models of this type are proposed, among others, by Guebeli *et al.* [11], Ide *et al.* [12, 13] and Shafai *et al.* [14]. The blackbox model of Ide is preferred here, as it reasonably describes the results of a series of experiments with metal V-belt CVTs [3, 4].

The steady state version of Ide's model yields a relation for the primary clamping force F_{p} that is required to maintain a given ratio r_{cvt} with a given secondary clamping force F_{s} and a given primary torque T_{p} (through the modified torque ratio τ_{s}'):

$$F_{\mathrm{p}} = \kappa(r_{\mathrm{cvt}}, \tau_{\mathrm{s}}') \cdot F_{\mathrm{s}} \tag{9}$$

For obvious reasons, the quantity κ in equation (9) is called the thrust ratio. Some experimentally obtained results for this highly non-linear function of the CVT ratio r_{cvt} and the torque ratio τ_{s}' are given in figure 5.

For instationary situations, Ide's model states that the rate of ratio change $\dot{r}_{\mathrm{cvt}}$ is a function of the ratio r_{cvt}, primary pulley speed ω_{p}, clamping forces F_{p} and F_{s} and torque ratio τ_{s}':

$$\dot{r}_{\mathrm{cvt}} = k_r(r_{\mathrm{cvt}}) \cdot |\omega_{\mathrm{p}}| \cdot F_{\mathrm{shift}}; \quad F_{\mathrm{shift}} = F_p - \kappa(r_{\mathrm{cvt}}, \tau_{\mathrm{s}}') \cdot F_{\mathrm{s}} \tag{10}$$

An axial force difference F_{shift}, weighted by the thrust ratio κ results in a ratio change, and is therefore called the shift force. The occurrence of ω_{p} in the model (10) is plausible because an increasing shift force is needed for decreasing pulley speeds to obtain the same rate of ratio change. The reason is that less V-shaped blocks enter the pulleys per second when the pulley speed decreases. As a result the radial belt travel per revolution of the pulleys must increase and this requires a higher shift force. However, it is far from obvious that the rate of ratio change is *proportional* to both the shift force and the primary pulley speed. k_r is a non-linear function of the ratio r_{cvt} and has been obtained experimentally. Experimental data has been used to obtain a piecewise linear fit, which are depicted in figure 6. The estimation of k_r has

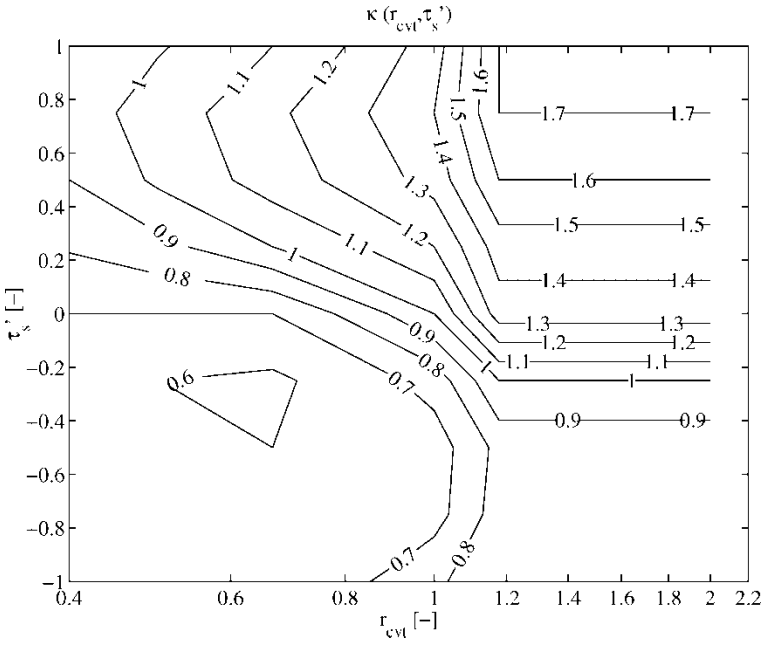

Figure 5. Contour plot of $\kappa(r_{\mathrm{cvt}}, \tau_{\mathrm{s}}')$.

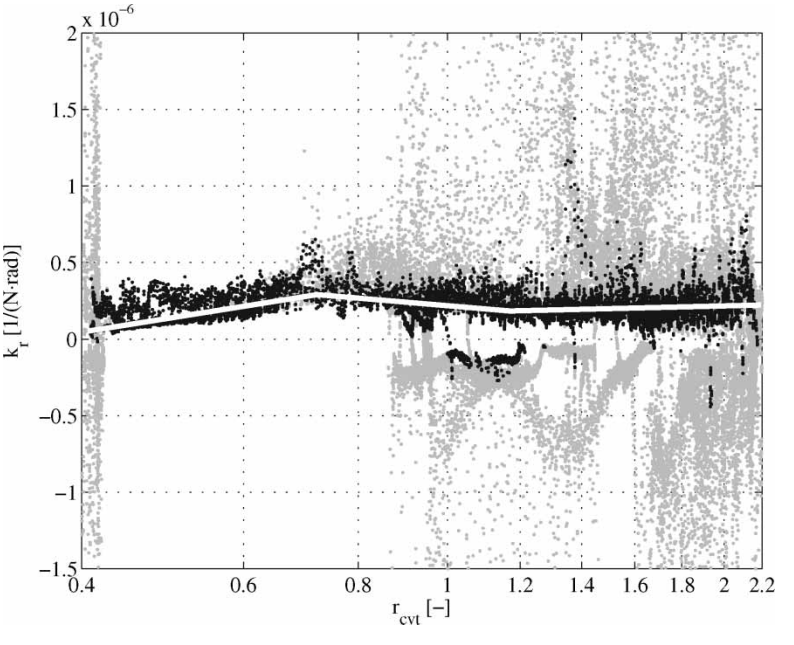

Figure 6. Fit of $k_r(r_{\mathrm{cvt}})$; greyed-out dots correspond to data with reduced accuracy.

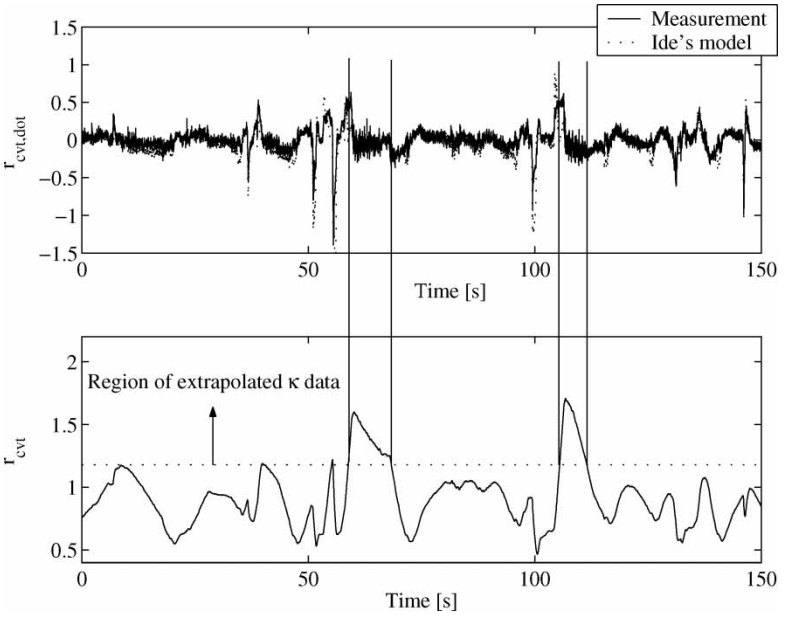

Figure 7. Comparison of shifting speed, Ide's model *vs.* measurement.

been obtained using the inverse Ide model:

$$k_r(r_{\text{cvt}}) = \frac{\dot{r}_{\text{cvt}}}{|\omega_{\text{p}}| \cdot F_{\text{shift}}} \tag{11}$$

In the denominator F_{shift} is present, the value of which can become (close to) zero. Obviously, the estimate is very sensitive for errors in F_{shift} when its value is small. The dominant disturbances in F_{shift} are caused by high-frequency pump generated pressure oscillations, which do not affect the ratio (due to the low-pass frequency behavior of unmodeled variator pulley inertias). The standard deviation of the pressure oscillations and other high-frequency disturbances has been determined applying a high-pass Butterworth filter to the data of F_{shift}. To avoid high-frequency disturbances in F_{shift} blurring the estimate of k_r, estimates for values of F_{shift} smaller than at least three times the disturbance's standard deviation have been ignored (these have been plotted as grey dots in figure 6), whereas the other points have been plotted as black dots. The white line is the resulting fit of this data. The few points with negative value for k_r have been identified as local errors in the map of κ.

To validate the quality of Ide's model, the shifting speed $\dot{r}_{\text{cvt}}$, recorded during a road experiment, is compared with the same signal predicted using the model. Model inputs are the hydraulic pulley pressures (p_{p}, p_{s}) and pulley speeds (ω_{p}, ω_{s}) together with the estimated primary pulley torque ($\hat{T}_{\text{p}}$). The result is depicted in figure 7. The model describes the shifting speed well, but for some upshifts it predicts too large values. This happens only for high CVT ratios, i.e. $r_{\text{cvt}} > 1.2$, where the data of κ is unreliable due to extrapolation (see figure 5).

3. The hydraulic system

The hydraulic part of the CVT (see figure 3) consists of a roller vane pump directly connected to the engine shaft, two solenoid valves and a pressure cylinder on each of the moving pulley

sheaves. The volume between the pump and the two valves including the secondary pulley cylinder is referred to as the secondary circuit, the volume directly connected to and including the primary pulley cylinder is the primary circuit. Excessive flow in the secondary circuit bleeds off toward the accessories, whereas the primary circuit can blow off toward the drain. All pressures are gage pressures, defined relative to the atmospheric pressure. The drain is at atmospheric pressure.

The clamping forces F_p and F_s are realized mainly by the hydraulic cylinders on the moveable sheaves and depend on the pressures p_p and p_s. As the cylinders are an integral part of the pulleys, they rotate with an often very high speed, so centrifugal effects have to be taken into account and the pressure in the cylinders will not be homogeneous. Therefore, the clamping forces will also depend on the pulley speeds ω_p and ω_s. Furthermore, a preloaded linear elastic spring with stiffness k_spr is attached to the moveable secondary sheave. This spring has to guarantee a minimal clamping force when the hydraulic system fails. Together this results in the following relations for the clamping forces:

$$F_\mathrm{p} = A_\mathrm{p} \cdot p_\mathrm{p} + c_\mathrm{p} \cdot \omega_\mathrm{p}^2 \tag{12}$$

$$F_\mathrm{s} = A_\mathrm{s} \cdot p_\mathrm{s} + c_\mathrm{s} \cdot \omega_\mathrm{s}^2 - k_\mathrm{spr} \cdot s_\mathrm{s} + F_0 \tag{13}$$

where c_p and c_s are constants, whereas F_0 is the spring force when the secondary moveable sheave is at position $s_\mathrm{s} = 0$. Furthermore, A_p and A_s are the pressurized piston surfaces. In the hydraulic system of figure 3, the primary pressure is smaller than the secondary pressure if there is an oil flow from the secondary to the primary circuit. Therefore, to guarantee that in any case the primary clamping force can be up to twice as large as the secondary clamping force, the primary piston surface A_p is approximately twice as large as the secondary surface A_s.

It is assumed that the primary and the secondary circuit are always filled with oil of constant temperature and a constant air fraction of 1%. The volume of circuit α ($\alpha = \mathrm{p}, \mathrm{s}$) is given by:

$$V_\alpha = V_{\alpha,\min} + A_\alpha \cdot s_\alpha \tag{14}$$

$V_{\alpha,\min}$ is the volume if $s_\alpha = 0$ and A_α is the pressurized piston surface.

The law of mass conservation, applied to the primary circuit, combined with equation (14), results in:

$$\kappa_\mathrm{oil} \cdot V_\mathrm{p} \cdot \dot{p}_\mathrm{p} = Q_\mathrm{sp} - Q_\mathrm{pd} - Q_\mathrm{p,leak} - Q_{\mathrm{p},V} \tag{15}$$

Q_sp is the oil flow from the secondary to the primary circuit, Q_pd is the oil flow from the primary circuit to the drain, $Q_\mathrm{p,leak}$ is the (relatively small) oil flow leaking through narrow gaps from the primary circuit and $Q_{\mathrm{p},V}$ is the oil flow due to a change in the primary pulley cylinder volume. Furthermore, κ_oil is the compressibility of oil. The oil flow Q_sp is given by:

$$Q_\mathrm{sp} = c_\mathrm{f} \cdot A_\mathrm{sp}(x_\mathrm{p}) \cdot \sqrt{\frac{2}{\rho} \cdot |p_\mathrm{s} - p_\mathrm{p}|} \cdot \mathrm{sign}(p_\mathrm{s} - p_\mathrm{p}) \tag{16}$$

where c_f is a constant flow coefficient and ρ is the oil density. A_sp, the equivalent valve opening area for this flow path, depends on the primary valve stem position x_p. Flow Q_pd follows from:

$$Q_\mathrm{pd} = c_\mathrm{f} \cdot A_\mathrm{pd}(x_\mathrm{p}) \cdot \sqrt{\frac{2}{\rho} \cdot p_\mathrm{p}} \tag{17}$$

Here, A_pd is the equivalent opening area of the primary valve for the flow from primary circuit to the drain. The construction of the valve implies that $A_\mathrm{sp}(x_\mathrm{p}) \cdot A_\mathrm{pd}(x_\mathrm{p}) = 0$ for all possible x_p.

Flow $Q_{\mathrm{p,leak}}$ is assumed to be laminar with leak flow coefficient c_{pl}, so:

$$Q_{\mathrm{p,leak}} = c_{\mathrm{pl}} \cdot p_{\mathrm{p}} \tag{18}$$

The flow due to a change of the primary pulley cylinder volume is described by:

$$Q_{\mathrm{p},V} = A_{\mathrm{p}} \cdot \dot{s}_{\mathrm{p}} \tag{19}$$

with $\dot{s}_{\mathrm{p}}$ given by equation (4).

Application of the law of mass conservation to the secondary circuit yields

$$\kappa_{\mathrm{oil}} \cdot V_{\mathrm{s}} \cdot p_{\mathrm{s}} = Q_{\mathrm{pump}} - Q_{\mathrm{sp}} - Q_{\mathrm{sa}} - Q_{\mathrm{s,leak}} - Q_{\mathrm{s},V} \tag{20}$$

The flow Q_{pump}, generated by the roller vane pump, depends on the angular speed ω_{e} of the engine shaft, on the pump mode m ($m = \mathrm{SS}$ for single sided and $m = \mathrm{DS}$ for double sided mode), and the pressure p_{s} at the pump outlet, so $Q_{\mathrm{pump}} = Q_{\mathrm{pump}}(\omega_{\mathrm{e}}, p_{\mathrm{s}}, m)$. Q_{sa} is the flow from the secondary circuit to the accessories and $Q_{\mathrm{s,leak}}$ is the leakage from the secondary circuit. Flow Q_{sa} is modeled as:

$$Q_{\mathrm{sa}} = c_{\mathrm{f}} \cdot A_{\mathrm{sa}}(x_{\mathrm{s}}) \cdot \sqrt{\frac{2}{\rho} \cdot |p_{\mathrm{s}} - p_{\mathrm{a}}|} \cdot \mathrm{sign}(p_{\mathrm{s}} - p_{\mathrm{a}}) \tag{21}$$

where A_{sa}, the equivalent valve opening of the secondary valve, depends on the valve stem position x_{s}. The laminar leakage flow $Q_{\mathrm{s,leak}}$ is given by (with flow coefficient c_{sl}):

$$Q_{\mathrm{s,leak}} = c_{\mathrm{sl}} \cdot p_{\mathrm{s}} \tag{22}$$

The flow due to a change of the secondary pulley cylinder volume is:

$$Q_{\mathrm{s},V} = A_{\mathrm{s}} \cdot \dot{s}_{\mathrm{s}} \tag{23}$$

with $\dot{s}_{\mathrm{s}}$ according to equation (3).

The accessory circuit contains several passive valves. In practice, the secondary pressure p_{s} will always be larger than the accessory pressure p_{a}, i.e. no backflow occurs. The relation between p_{a} and p_{s} is approximately linear, so

$$p_{\mathrm{a}} = c_{\mathrm{a0}} + c_{\mathrm{a1}} \cdot p_{\mathrm{s}} \tag{24}$$

with constants $c_{\mathrm{a0}} > 0$ and $c_{\mathrm{a1}} \in (0, 1)$.

Now that a complete model of the pushbelt CVT and its hydraulics is available, the controller and its operational constraints can be derived.

4. The constraints

The CVT ratio controller (in fact) controls the primary and secondary pressures. Several pressure constraints have to be taken into account by this controller:

1. the torque constraints $p_{\alpha} \geq p_{\alpha,\mathrm{torque}}$ to prevent slip on the pulleys;
2. the lower pressure constraints $p_{\alpha} \geq p_{\alpha,\mathrm{low}}$ to keep both circuits filled with oil. Here, fairly arbitrary, $p_{\mathrm{p,low}} = 3$ [bar] is chosen. To enable a sufficient oil flow Q_{sa} to the accessory circuit, and for a proper operation of the passive valves in this circuit it is necessary that

Q_{sa} is greater than a minimum flow $Q_{sa,min}$. A minimum pressure $p_{s,low}$ of 4 [bar] turns out to be sufficient;
3. the upper pressure constraints $p_\alpha \leq p_{\alpha,max}$, to prevent damage to the hydraulic lines, cylinders and pistons. Hence, $p_{p,max} = 25$ [bar], $p_{s,max} = 50$ [bar];
4. the hydraulic constraints $p_\alpha \geq p_{\alpha,hyd}$ to guarantee that the primary circuit can bleed off fast enough toward the drain and that the secondary circuit can supply sufficient flow toward the primary circuit.

The pressures $p_{p,torque}$ and $p_{s,torque}$ in constraint 1 depend on the critical clamping force F_{crit}, equation (5). The estimated torque $\hat{T}_p$ is calculated using the stationary engine torque map, torque converter characteristics and lock-up clutch mode, together with inertia effects of the engine, flywheel and primary gearbox shaft. A safety factor $k_s = 0.3$ with respect to the estimated maximal primary torque $\hat{T}_{p,max}$ has been introduced to account for disturbances on the estimated torque $\hat{T}_p$, such as shock loads at the wheels. Then the pulley clamping force (equal for both pulleys, neglecting the variator efficiency) needed for torque transmission becomes:

$$F_{torque} = \frac{\cos(\varphi) \cdot (|\hat{T}_p| + k_s \cdot \hat{T}_{p,max})}{2 \cdot \mu \cdot R_p} \tag{25}$$

Consequently, the resulting pressures can be easily derived using equations (12) and (13):

$$p_{p,torque} = \frac{1}{A_p}\left(F_{torque} - c_p \cdot \omega_p^2\right) \tag{26}$$

$$p_{s,torque} = \frac{1}{A_s}\left(F_{torque} - c_s \cdot \omega_s^2 - k_{spr} \cdot s_s - F_0\right) \tag{27}$$

Exactly the same clamping strategy has been previously used by ref. [3] during test stand efficiency measurements of this gearbox and test vehicle road tests. No slip has been reported during any of those experiments. As the main goal of this work is to an improved ratio tracking behavior, the clamping strategy has remained unchanged.

A further elaboration of constraints 4 is based on the law of mass conservation for the primary circuit. First of all, it is noted that for this elaboration the leakage flow $Q_{p,leak}$ and the compressibility term $\kappa_{oil} \cdot V_p \cdot \dot{p}_p$ may be neglected because they are small compared to the other terms. Furthermore, it is mentioned again that the flows Q_{sp} and Q_{pd} can never be unequal to zero at the same time. Finally, it is chosen to replace the rate of ratio change $\dot{r}_{cvt}$ by the desired rate of ratio shift $\dot{r}_{cvt,d}$, that is specified by the hierarchical driveline controller. If $\dot{r}_{cvt,d} < 0$, then oil has to flow out of the primary cylinder to the drain, so $Q_{pd} > 0$ and $Q_{sp} = 0$. Constraint 4 with respect to the primary pulley circuit then results in the following relation for the pressure $p_{p,hyd}$:

$$p_{p,hyd} = \frac{\rho_{oil}}{2} \cdot \left(\frac{A_p \cdot \nu_p \cdot \max(0, -\dot{r}_{cvt,d})}{c_f \cdot A_{pd,max}}\right)^2 \tag{28}$$

where $A_{pd,max}$ is the maximum opening of the primary valve in the flow path from the primary cylinder to the drain.

In a similar way, a relation for the secondary pulley circuit pressure $p_{s,hyd}$ in constraint 4 can be derived. This constraint is especially relevant if $\dot{r}_{cvt} > 0$, i.e. if the flow Q_{sp} from the secondary to the primary circuit has to be positive and, as a consequence, $Q_{pd} = 0$. This then

results in:

$$p_{\mathrm{s,hyd}} = p_{\mathrm{p,d}} + \frac{\rho_{\mathrm{oil}}}{2} \cdot \left(\frac{A_{\mathrm{p}} \cdot \nu_{\mathrm{p}} \cdot \max(0, \dot{r}_{\mathrm{cvt,d}})}{c_{\mathrm{f}} \cdot A_{\mathrm{sp,max}}} \right)^2 \tag{29}$$

where $A_{\mathrm{sp,max}}$ is the maximum opening of the primary valve in the flow path from the secondary to the primary circuit.

For the design of the CVT ratio controller it is advantageous to reformulate to constraints in terms of clamping forces instead of pressures. Associating a clamping force $F_{\alpha,\beta}$ with the pressure $p_{\alpha,\beta}$ and using equations (12) and (13) this results in the requirement:

$$F_{\alpha,\mathrm{min}} \leq F_{\alpha} \leq F_{\alpha,\mathrm{max}} \tag{30}$$

with minimum pulley clamping forces:

$$F_{\alpha,\mathrm{min}} = \max(F_{\alpha,\mathrm{low}}, F_{\alpha,\mathrm{torque}}, F_{\alpha,\mathrm{hyd}}) \tag{31}$$

5. Control design

It is assumed in this section that at each point of time t, the primary speed $\omega_{\mathrm{p}}(t)$, the ratio $r_{\mathrm{cvt}}(t)$, the primary pressure $p_{\mathrm{p}}(t)$ and the secondary pressure $p_{\mathrm{s}}(t)$ are known from measurements, filtering and/or reconstruction. Furthermore, it is assumed that the CVT is mounted in a vehicular driveline and that the desired CVT ratio $r_{\mathrm{cvt,d}}(t)$ and the desired rate of ratio change $\dot{r}_{\mathrm{cvt,d}}(t)$ are specified by the overall hierarchical driveline controller. This implies, for instance, that at each point of time the constraint forces can be determined.

The main goal of the local CVT controller is to achieve fast and accurate tracking of the desired ratio trajectory. Furthermore, the controller should also be robust for disturbances. An important subgoal is to maximize the efficiency. It is quite plausible (and otherwise supported by experiments, [3]) that to realize this sub-goal the clamping forces F_{p} and F_{s} have to be as small as possible, taking the requirements in equation (30) into account.

The output of the ratio controller is subject to the constraints of equation (31). The constraints $F_{\alpha} \geq F_{\alpha,\mathrm{min}}$ can effectively raise the clamping force setpoint of one pulley, resulting in an undesirable ratio change. This can be counteracted by raising the opposite pulley's clamping force as well, using model-based compensator terms in the ratio controller. Using Ide's model, i.e. using equation (10), expressions for the ratio change forces $F_{\mathrm{p,ratio}}$ and $F_{\mathrm{s,ratio}}$ (figure 8) can be easily derived:

$$F_{\mathrm{p,ratio}} = F_{\mathrm{shift,d}} + \kappa \cdot F_{\mathrm{s,min}} \tag{32}$$

$$F_{\mathrm{s,ratio}} = \frac{-F_{\mathrm{shift,d}} + F_{\mathrm{p,min}}}{\kappa} \tag{33}$$

where $F_{\mathrm{shift,d}}$ is the desired shifting force, basically a weighted force difference between both pulleys. As explained earlier, κ depends on τ_{s}', which in turn depends on F_{s}. This is an implicit relation ($F_{\mathrm{s,ratio}}$ depends on F_{s}), which has been tackled by calculating κ from pressure measurements.

It will now be shown that at each time, one of the two clamping forces is equal to $F_{\alpha,\mathrm{min}}$, whereas the other determines the ratio. Using equations (30), (32) and (33) the desired primary

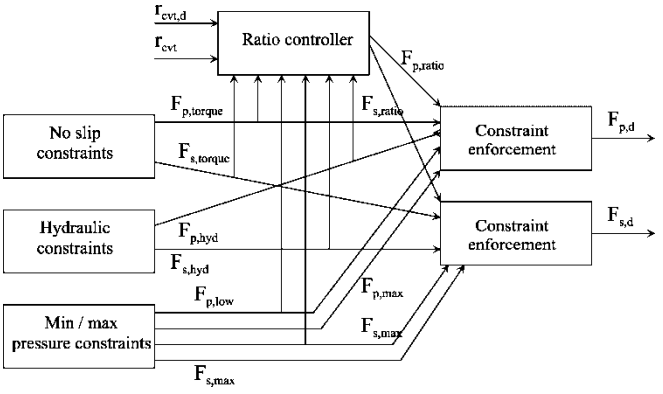

Figure 8. Ratio controller with constraints compensation

and secondary clamping forces $F_{\mathrm{p,d}}$ and $F_{\mathrm{s,d}}$ are given by:

$$\left.\begin{aligned} F_{\mathrm{p,d}} &= F_{\mathrm{p,ratio}} \\ F_{\mathrm{s,d}} &= F_{\mathrm{s,min}} \end{aligned}\right\} \quad \text{if } F_{\mathrm{shift,d}} + \kappa \cdot F_{\mathrm{s,min}} > F_{\mathrm{p,min}} \tag{34}$$

$$\left.\begin{aligned} F_{\mathrm{p,d}} &= F_{\mathrm{p,min}} \\ F_{\mathrm{s,d}} &= F_{\mathrm{s,ratio}} \end{aligned}\right\} \quad \text{if } F_{\mathrm{shift,d}} + \kappa \cdot F_{\mathrm{s,min}} < F_{\mathrm{p,min}} \tag{35}$$

In fact, the ratio is controlled in such a way that the shifting force F_{shift} becomes equal to $F_{\mathrm{shift,d}}$. For the resulting shifting force holds $F_{\mathrm{shift}} = F_{\mathrm{p,d}} - \kappa \cdot F_{\mathrm{s,d}}$, so:

$$F_{\mathrm{shift}} = \begin{cases} F_{\mathrm{p,ratio}} - \kappa \cdot F_{\mathrm{s,min}} = F_{\mathrm{shift,d}} & \text{if } F_{\mathrm{shift,d}} + \kappa \cdot F_{\mathrm{s,min}} > F_{\mathrm{p,min}} \\ F_{\mathrm{p,min}} - \kappa \cdot F_{\mathrm{s,ratio}} = F_{\mathrm{shift,d}} & \text{if } F_{\mathrm{shift,d}} + \kappa \cdot F_{\mathrm{s,min}} < F_{\mathrm{p,min}} \end{cases} \tag{36}$$

This holds as long as the clamping forces do not saturate on their maximum constraint ($F_{\alpha,\mathrm{ratio}} \leq F_{\alpha,\mathrm{max}}$). In the case of $F_{\alpha,\mathrm{ratio}} \geq F_{\alpha,\mathrm{max}}$, $F_{\alpha,\mathrm{d}} = F_{\alpha,\mathrm{max}}$, $F_{\mathrm{shift}} \neq F_{\mathrm{shift,d}}$. Hence, the shifting speed is limited because of actuator saturation.

To complete the controller, $F_{\mathrm{shift,d}}$ must be specified. As the dynamics of the variator (according to Ide's model) are quite non-linear, an equivalent input u is introduced, using an inverse representation of the Ide model for $F_{\mathrm{shift,d}}$:

$$F_{\mathrm{shift,d}} = \frac{u + \dot{r}_{\mathrm{cvt,d}}}{k_r \cdot |\omega_{\mathrm{p}}|} \tag{37}$$

Basically a feedback-linearizing weighting of u with the reciprocal of both $|\omega_{\mathrm{p}}|$ and k_r is applied. This cancels the (known) non-linearities in the variator, see, e.g. Slotine *et al.* [15]. Further, a setpoint feedforward is introduced, which will reduce the phase lag of the controlled system responses.

Owing to model inaccuracies or due to external disturbances unaccounted for (like the upper clamping force constraints), differences γ between $\dot{r}_{\mathrm{cvt}}$ and $\dot{r}_{\mathrm{cvt,d}}$ will occur:

$$\dot{r}_{\mathrm{cvt}} = \dot{r}_{\mathrm{cvt,d}} + u + \gamma \tag{38}$$

Good tracking behavior is obtained if u cancels γ well. A linear feedback controller has been chosen for u based on the knowledge that (contrary to equation (10)), there are inertias involved, requiring at least a second order controller. Consequently, a PID controller is used.

The proportional action is necessary for a rapid reduction of errors, whereas the integrating action is needed in order to track ramp ratio setpoints with zero error. Some derivative action proved necessary to gain larger stability margins (and less oscillatory responses). The controller is implemented as follows:

$$u = P \cdot (r_{\text{cvt,d}} - r_{\text{cvt}}) + I \cdot \int_0^t \left[k_{\text{e}} \cdot (r_{\text{cvt,d}} - r_{\text{cvt}})\right] \mathrm{d}\tau + D \cdot \dot{r}_{\text{cvt}} \tag{39}$$

where $k_{\text{e}} \in \{0, 1\}$ switches the integrator on and off depending on certain conditions that are explained further on. The derivative action of the controller only acts on the measured CVT ratio signal to avoid an excessive controller response on stepwise changes of the ratio setpoint. Additionally, a high-frequency pole has been added to the derivative operation to prevent excessive gains at high frequencies. The controller parameters P, I and D have been tuned manually.

During instances of actuator saturation (because of the maximum force constraints), the closed loop is effectively broken (measurement r_{cvt} does not react to changes in u anymore). This will lead to degraded performance, as the value of the controller's integrator continues to grow. This so-called integrator windup is undesirable. A conditional anti-windup mechanism has been added to limit the integrator's value during saturation:

$$k_{\text{e}} = \begin{cases} 1 & \text{if } F_{\text{p,ratio}} \leq F_{\text{p,max}} \wedge F_{\text{s,ratio}} \leq F_{\text{s,max}} \\ 0 & \text{if } F_{\text{p,ratio}} > F_{\text{p,max}} \vee F_{\text{s,ratio}} > F_{\text{s,max}} \end{cases} \tag{40}$$

If either pressure saturates ($p_{\text{p}} = p_{\text{p,max}}$ or $p_{\text{s}} = p_{\text{s,max}}$), the shifting speed error γ inevitably becomes large. The anti-windup algorithm ensures stability, but the tracking behavior will deteriorate. This is a hardware limitation which can only be tackled by enhancing the variator and hydraulics hardware. The advantage of a conditional anti-windup *vs.* a standard (linear) algorithm is that the linear approach requires tuning for good performance, whereas the conditional approach does not. Furthermore, the performance of the conditional algorithm closely resembles that of a well-tuned linear mechanism.

6. Experimental results

As the CVT is already implemented in a test vehicle, in-vehicle experiments on a roller bench have been performed to tune and validate the new ratio controller. To prevent a non-synchronized operation of throttle and CVT ratio, the accelerator pedal signal (see figure 1) has been used as the input for the validation experiments. The coordinated controller will track the maximum engine efficiency operating points. A semi kick-down action at a cruise-controlled speed of ~50 km/h followed by a pedal back out has been performed in a single reference experiment. The recorded pedal angle (see figure 9) has been applied to the coordinated controller. This approach cancels the limited human driver's repeatability.

The upper plot of figure 10 shows the CVT ratio response calculated from speed measurements using equation (1), the plot depicts the tracking error. As this is a quite demanding experiment, the tracking is still adequate. Much better tracking performance can be obtained with more smooth setpoints, but the characteristics of the responses will become less distinct as well. Figure 11 shows the primary and secondary pulley pressures. The initial main peak in the error signal (around $t = 1.5$ s) is caused by saturation of the secondary pressure (lower plot of figure 11), due to a pump flow limitation. If a faster initial response were required, adaptation of the hydraulics hardware would be necessary. After the initial fast downshift, the ratio reaches its setpoint (around $t = 7$ s) before downshifting again. All changes in shifting

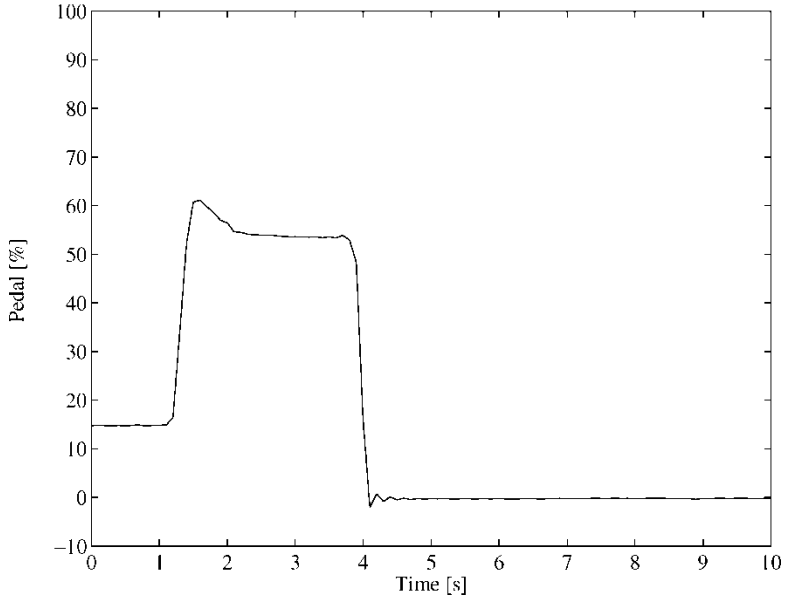

Figure 9. Pedal input for the CVT powertrain.

direction ($t = 1.3$, $t = 1.6$ and $t = 7.5$ s) occur with a relatively small amount of overshoot, which shows that the integrator anti-windup algorithm performs well.

Looking at the primary pressure in the vicinity of $t = 1.5$ s, it can be observed that this pressure peaks repeatedly above its setpoint. This behavior is caused by performance limitations of the primary pressure controller. The developed controller guarantees that only one pulley pressure setpoint at the time is raised above its lower constraint, and only to realize

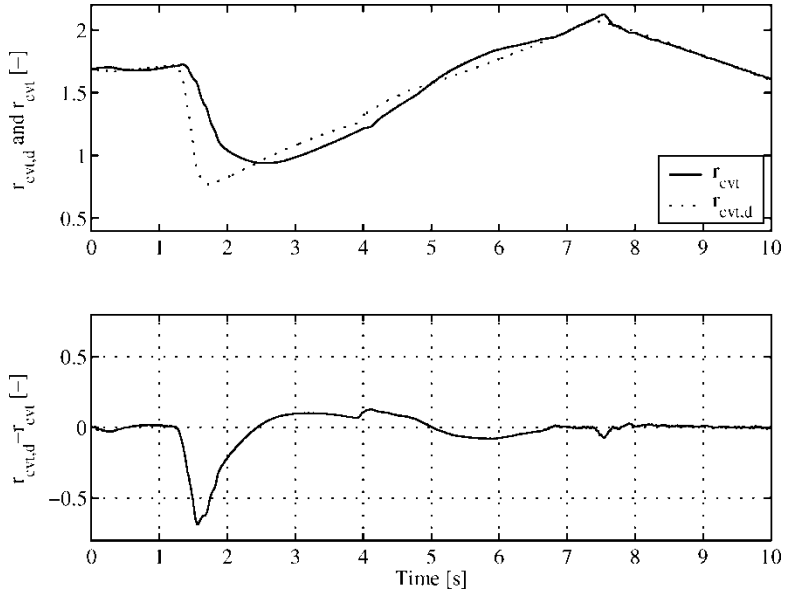

Figure 10. CVT ratio response and tracking error, roller bench semi-kickdown.

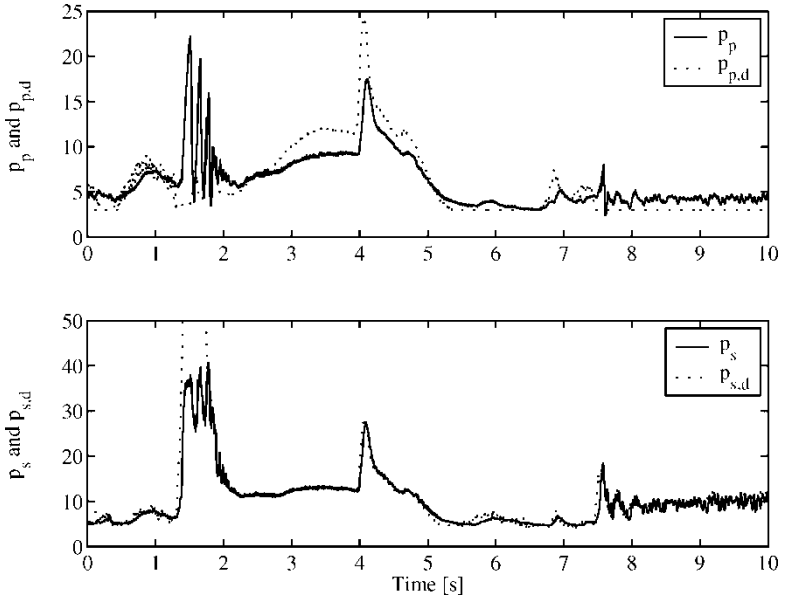

Figure 11. Primary and secondary pulley pressures, roller bench semi-kickdown.

a desired ratio. This is visualized in figure 12. Higher clamping forces cause more losses in the CVT [10], as long as no macro-slip occurs. The main causes are oil pump power demand (approximately linear with pressure) and losses in the belt itself, which both increase with increasing clamping pressure, as supported by measurements [16]. Hence, this controller has a potential for improving the efficiency of a CVT, compared to non-model based controllers.

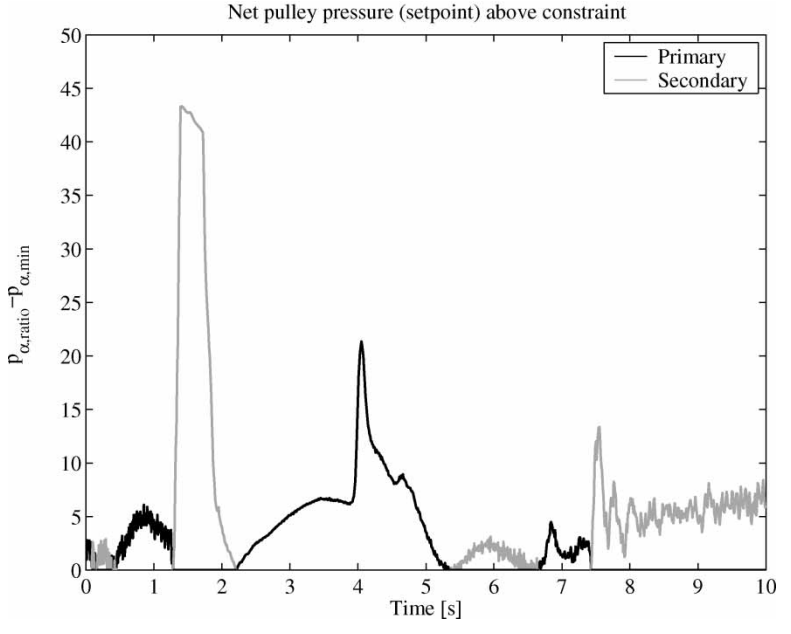

Figure 12. New controller's pulley pressure setpoints minus lower constraints.

Looking back to the lower plot of figure 10, the second (positive) peak (after the first negative peak due to actuator saturation) represents the overshoot of the ratio response due to a shifting direction change. This quantity describes the tracking performance of a controller well, and will be used to evaluate a controller's performance. The overshoot is computed here as the (positive) maximum of the ratio error: $\max(r_{\mathrm{cvt,d}} - r_{\mathrm{cvt}})$. Also, the mean absolute error $(1/N)\sum_0^N |r_{\mathrm{cvt,d}} - r_{\mathrm{cvt}}|$ (for the N data points in the 10 s response) will be used to compare results.

The same experiment has been performed for several variations on the controller. For each of these variations, all constraints are still imposed, but some of the compensator terms in the ratio controller have been temporarily switched off (the vertical arrows in figure 8). The results have been compared with the results for the total controller and are depicted in figure 13. The cases that will be addressed are:

1. All feedforwards and compensators on ('total').
2. No setpoint feedforward ('setp ff off'), $\dot{r}_{\mathrm{cvt,d}} = 0$ in equation (37).
3. No critical (no belt slip) torque constraint compensation ('T comp off'), $F_{\mathrm{torque}} = 0$.
4. No hydraulic constraints compensation ('hydr comp off'), $F_{\alpha,\mathrm{hyd}} = 0$.
5. No torque transmission nor hydraulic constraints compensation ('T,hydr comp off'), $F_{\mathrm{torque}} = 0$, $F_{\alpha,\mathrm{hyd}} = 0$.

It is immediately clear that of all alternatives, the total controller with all feedforwards and compensators on ('total') described in the previous paragraph performs best, implying that all controller terms have a positive contribution towards minimizing the tracking error. Switching off either the hydraulic constraints compensation terms ('hydr comp off') or the torque transmission compensator ('T comp off') does not severely degrade the tracking quality. However, switching both compensators off ('T,hydr comp off') does introduce large tracking errors. This occurs because the maximum operator of both constraints is taken to calculate the compensating action, and if one constraint compensator is zero, the output of the maximum operator

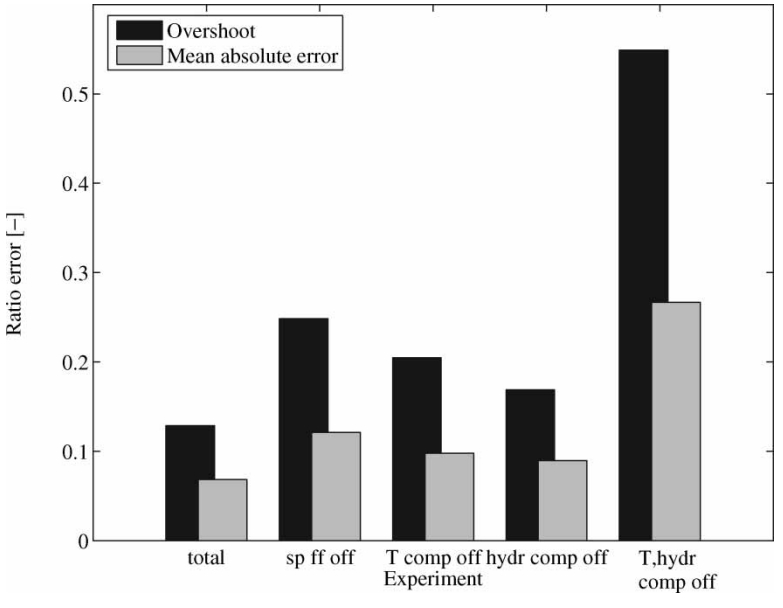

Figure 13. Overshoot and mean absolute error for several controller alternatives.

will still be non-zero due to the second constraint. Both compensators switched off simultaneously effectively introduce a 'dead zone' in the controller output u, the result of which is obvious. The response with the setpoint feedforward switched off ('setp ff off') increases the errors due to increased phase lag of the resulting response. The obtained results of the total developed controller show better tracking behavior (overshoot and mean absolute error) and lower transient pulley pressures (only during ratio change, as the clamping strategy is equal) compared with results obtained with a previously adopted controller, as described in ref. [3]. This could be an indication for the potential for improving the CVT efficiency of the new controller, as described before.

Vehicle tests including tip shifting (featuring stepwise ratio setpoint changes) have been performed on a test track, see figure 14. The stepwise changes in the ratio setpoint are trajectories that cannot be realized. Hence, the measured CVT ratio will always lag behind. Hence, this experiment demonstrates the robustness against actuator saturation, as the pressure of the pulley that controls the ratio will saturate. As the errors in the feedforward terms of the controller will increase, the feedback controller becomes increasingly important. Also the anti-windup mechanism of the ratio controller needs to prevent overshoot. Results of an experiment driving at a cruise-controlled speed of 50 km/h are depicted in figures 15 and 16. A new gear ratio setpoint is generated every 2 s.

At the start of the up-shift ratio responses at $t = 2.1$ s and $t = 4.2$ s, an inverse response is present. As the shifting speeds are indeed very high in this experiment, because of the layout of the hydraulic system, the secondary circuit needs to supply the primary circuit with oil. As a result, the secondary pressure rises in advance to the primary pressure and causes an initial downshift. Around $t = 3$ s and $t = 5$ s, the ratio initially rises approximately linear, caused by the limited pump flow as the oil pump runs at engine speed, which is low. Upshifting is further characterized by some overshoot, which is clearly visible at $t = 14$ s. As the primary pressure cannot drop sufficiently quick due to a limited primary valve flow-through area toward the drain, upshifting continues and causes overshoot. The secondary pressure only saturates briefly due to the limited pump flow after each ratio setpoint change. Much less overshoot is present during a downshift, the speed of which is not limited by pump flow. Again the primary pressure peaks above its setpoint when the secondary pressure is increased rapidly, caused

Figure 14. Experimental vehicle during tip-shifts at the test track.

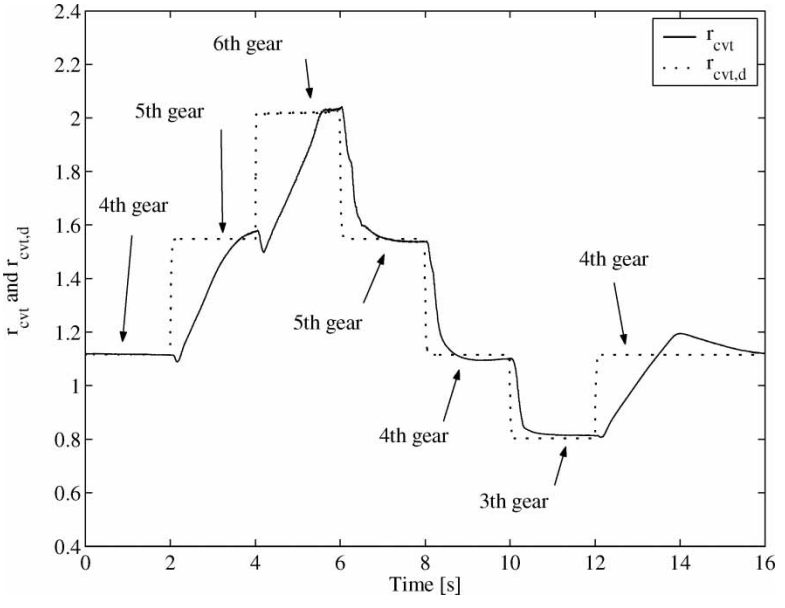

Figure 15. CVT ratio response and tracking error, road tip shifting.

by limitations in the primary pressure controller. This phenomenon lowers the maximum downshift speed and is visible as a slight 'bump' in the ratio at $t = 6.2$ s and $t = 8.2$ s.

As the main goal of the presented experiments is to demonstrate a new ratio controller concept, during the experiments belt slip has been avoided using a proven clamping strategy as mentioned earlier. Also, an online model-based detection algorithm was used, verifying that $|\tau_s'| \leq 1$. Two methods to detect belt slip off-line from measurement data (without direct

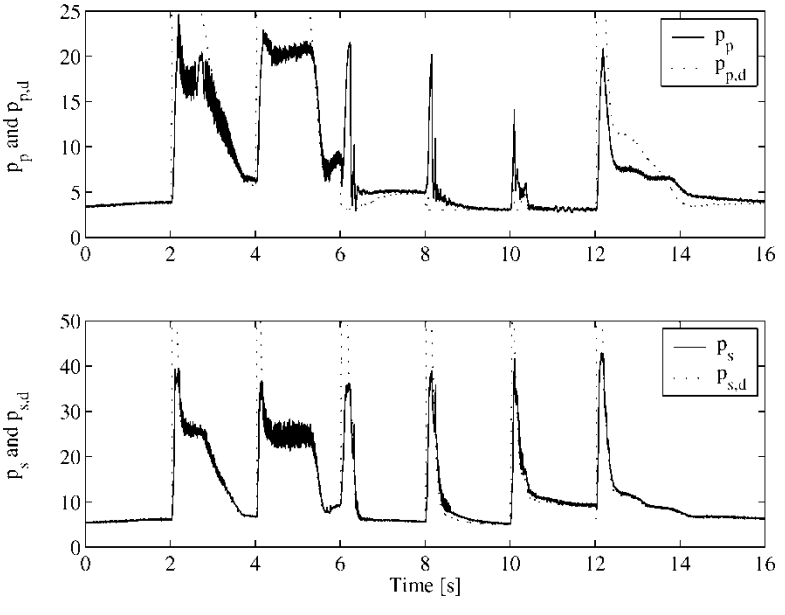

Figure 16. Primary and secondary pulley pressures, road tip shifting.

measurements of the belt's running radius on the pulleys to calculate the so-called geometric ratio) have been used after the experiments. First, it has been verified if the range of CVT ratios geometrically possible is not exceeded ($r_{\mathrm{LOW}} \leq r_{\mathrm{cvt}} \leq r_{\mathrm{OD}}$). Secondly, the maximum shifting speed of the CVT is limited due to limited clamping forces and variator speed, see equation (10). The coefficient of friction in the excessive (macro-) slip region of a push-belt decreases with slip speed [8]. This causes unstable dynamic behavior, and hence slip speed will increase rapidly when the torque capacity of a V-belt is exceeded. As the ratio is calculated from measured pulley speeds, excessively fast ratio changes (high values of $\dot{r}_{\mathrm{cvt}}$) can indicate belt slip. The results of each measurement have been scrutinized, the result of which did not show any traces of belt slip effects.

7. Conclusions

A new ratio controller for a metal push-belt CVT with a hydraulic belt clamping system has been developed. On the basis of dynamic models of the variator and hydraulics, compensator terms of system constraints, a setpoint feedforward and a linearizing feedback controller have been implemented. The feedback controller is a PID controller with conditional anti-windup protection. The total ratio controller guarantees that, at least one of the pressure setpoints is always minimal with respect to its constraints, while the other is raised above the minimum level to enable shifting. This approach has potential for a CVT efficiency inprovement. Roller bench and road experiments with a vehicle built-in CVT show that adequate tracking is obtained. The largest deviations from the ratio setpoint are caused by actuator pressure saturation. Experiments with several controller variations featuring feedforwards being switched off reveal that all implemented feedforward and constraint compensator terms have a beneficial effect on minimizing the tracking error. Tip shift experiments revealed good robustness against actuator saturation.

References

[1] Frank, A.A. and Francisco, A., 2002, Ideal operating line CVT shifting strategy for hybrid electric vehicles. *Proceedings of the International Congress on Continuously Variable Power Transmission (CVT'02)*, VDI Berichte 1709, pp. 211–227.

[2] Ozeki, T. and Umeyama, M., 2002, Development of Toyota's transaxle for mini-van hybrid vehicles. *Transmission and Driveline Systems Symposium 2002*, SP-1655, no. 2002-01-0931.

[3] Vroemen, B.G., 2001, Component control for the zero inertia powertrain. PhD thesis, Technische Universiteit Eindhoven, The Netherlands.

[4] Stouten, B., 2000, Modeling and control of a CVT. WFW-Report 2000.10, Technische Universiteit Eindhoven, The Netherlands.

[5] Spijker, E., 1994, Steering and control of a CVT based hybrid transmission for a passenger car. PhD thesis, Technische Universiteit Eindhoven, The Netherlands.

[6] van der Laan, M. and Luh, J., 1999, Model-based variator control applied to a belt type CVT. *Proceedings of the International Congress on Continuously Variable Power Transmission (CVT'99)*, Eindhoven, The Netherlands, pp. 105–110.

[7] Vanvuchelen, P., 1997, Virtual engineering for design and control of continuously variable transmissions. PhD, thesis, Katholieke Universiteit Leuven, Belgium.

[8] van Drogen, M. and van der Laan, M., 2003, Determination of variator robustness under macro slip conditions for a push belt CVT. *SAE paper* 2003-01-0480.

[9] Lee, H. and Kim, H., 2000, Analysis of primary and secondary thrusts for a metal belt CVT; Part 1: New relation considering band tension and block compression. *SAE paper* 2000-01-0841.

[10] Bonsen, B., Klaassen, T.W.G.L., van de Meerakker, K.G.O., Steinbuch, M. and Veenhuizen, P.A., 2003, Analysis of slip in a continuously variable transmission. *Proceedings of the 2003 ASME International Mechanical Engineering Congress (IMECE'03)*, Washington, DC., November 15–21.

[11] Guebeli, M, Micklem, J.D. and Burrows, C.R., 1993, Maximum transmission efficiency of a steel belt continuously variable transmission. *Transactions of the ASME Journal of Mechanical Design*, **115**, 1044–1048.

[12] Ide, T., Udagawa, A. and Kataoka, R., 1994, A dynamic response analysis of a vehicle with a metal V-belt CVT. *Proceedings of the Second International Symposium on Advanced Vehicle Control (AVEC'94)*, Tsukuba, Japan, Vol. 1, 230–235.

[13] Ide, T., Udagawa, A. and Kataoka, R., 1996, Experimental investigation on shift-speed characteristics of a metal V-belt CVT. *Proceedings of the International Congress on Continuously Variable Power Transmission (CVT'96)*.

[14] Shafai, E., Simons, M., Neff, U. and Geering, H.P., 1995, Model of a continuously variable transmission. *Proceedings of the First IFAC Workshop on Advances in Automotive Control*, pp. 99–107.

[15] Slotine, J.-J. E. and Li, W., 1991, Applied Nonlinear Control. ISBN 0-13-040890-5 (Englewood Cliffs, NJ: Prentice-Hall).

[16] Ide, T., 1999, Effect of power losses of metal V-belt CVT components on the fuel economy. CVT. *Proceedings of the International Congress on Continuously Variable Power Transmission (CVT'99)*, Eindhoven, The Netherlands, pp. 93–98.